Mass Transfer at the Solid-Liquid Interface for Climbing Film Flow in an Annular Duct

A. M. SUTEY and J. G. KNUDSEN

Oregon State University, Corvallis, Oregon

A method utilizing a diffusion controlled electrochemical reaction was used to measure average and instantaneous mass transfer coefficients at the solid-liquid interface in upward gas-liquid climbing film flow in a vertical annular duct. These measurements give some indication of the mechanics of flow of the film, the extent of turbulence at the inner wall, and the effect of film thickness and wave motion on the mass transfer process at the inner wall. Predictions of incipient downflow of the film, shear stress at the inner wall, and interfacial shear stress were obtained from these measurements. Fluctuations in the velocity gradient at the inner wall were also studied. Results of this study are in good agreement with previous work and with theoretical predictions based on simplified momentum balance concepts.

Climbing film flow is but one of the various regimes of upward two-phase (gas-liquid) flow. In climbing film flow the liquid moves upward as a film on the surface of the duct as the faster moving gas stream flows upward adjacent to the liquid film. Due to the momentum transfer at the gas-liquid interface, the liquid film is transported upward at the expense of the pressure energy of the gas stream. As a result, the liquid film is characterized by complex wave and entrainment phenomena. This type of flow is of particular interest since it exists over a rather wide range of gas and liquid flow rates and is commonly encountered in process equipment.

A knowledge of the mechanics of climbing film flow is essential to predict and understand the momentum, heat, and mass transfer processes which occur in the process. However, the difficulties involved in determining the fluid dynamics of the climbing film are considerable, primarily, since it is nearly impossible to probe the thin film without disturbing it. Theoretical models of the climbing film can be tested better by means of accurate local measurements than by the total liquid flow approach which has been employed in many investigations.

In the present study, the liquid flows as a film up the concentric inner core of an annulus while air flows upward in the annular space, the outer wall of the annulus remaining dry. Such an arrangement permits direct observation of the climbing film through a transparent outer tube and simplifies the measurement of pressure gradients, air velocity profiles, and film structure.

An electrochemical method utilizing a diffusion controlled ferro-ferricyanide redox couple was used to measure average and instantaneous mass transfer coefficients at the solid-liquid film interface. This method has been used extensively in various geometrical systems by many investigators (*1, 2, 6, 8, 12, 16* to *18, 20* to *24*), but has been restricted to oxygen-free systems. A preliminary study was performed by us (*26, 27*) in a pipe flow system to measure the actual effect of dissolved oxygen on the measured mass transfer coefficient. It was found that the electrochemical technique can be applied in the presence of air if certain precautions are taken.

This study demonstrates the advantage of local instantaneous measurements in describing climbing film phenomena. Further studies of this type will lead to a more basic understanding of the processes of heat, mass, and momentum transfer which occur in two-phase gas-liquid film flow.

BACKGROUND THEORY

Detailed theory relating to the measurement of mass transfer coefficients by the electrochemical method is given elsewhere (*26, 27*). The simplified current equation is:

$$\frac{i}{An\ F} = \bar{k}_c\,(c_b - c_w) \tag{1}$$

At the limiting current the interfacial concentration c_w becomes zero, and the rate of mass transfer is expressed as

$$\frac{i_L}{An\ F} = \bar{k}_c\, c_b \tag{2}$$

where $\bar{k}_c$ is the mass transfer coefficient and is a function of Reynolds number, Schmidt number, and geometry. Typical polarization curves for the ferro-ferricyanide system are shown in Figure 4. Limiting current is obtained at the flat portion of the curve. The occurrence of a limiting current confirms that the reaction is diffusion controlled. In this manner, experimental mass transfer coefficients can be determined from Equation (2). It should be noted that this development does not require the existence of any special type of fluid dynamics near the electrode surface.

Momentum Transfer in Climbing Film Flow

In our investigation the liquid film flows upward on the inner concentric core of an annulus as shown in Figure 1. The simplified steady state equations of continuity and momentum for the climbing film flow system are:

$$\frac{\rho u}{g_c}\frac{\partial u}{\partial x} = \frac{-\partial P}{\partial x} + \frac{1}{r}\frac{\partial}{\partial r}(r\tau) - \frac{\rho g}{g_c} \tag{3}$$

A. M. Sutey is with Batelle Northwest, Richland, Washington.

$$0 = \frac{\partial P}{\partial r} \tag{4}$$

$$0 = \frac{\partial u}{\partial x} + \frac{1}{r}\frac{\partial (rv)}{\partial r} \tag{5}$$

If we assume that $\partial P/\partial x$ is constant; the liquid film is of uniform thickness, r_i; no mass transfer occurs between the gas and the liquid either by diffusion or entrainment; and physical properties are constant, we may obtain the following expressions:

$$\frac{dP}{dx}\int_1^2 rdr + \frac{\rho g}{g_c}\int_1^2 rdr + \frac{\rho}{g_c}\int_1^2 u\frac{du}{dx}rdr = [r\tau]_1^2$$

$$\frac{dP}{dx} + \frac{\rho g}{g_c} + \frac{(\rho/g_c)}{(r_2^2 - r_1^2)}\frac{d}{dx}\int_1^2 u^2 rdr = \frac{2[r\tau]_1^2}{(r_2^2 - r_1^2)} \tag{6}$$

Applying Equation (6) to various regions of the annulus, one may obtain the following shear stress relationships, assuming that kinetic energy effects are negligible compared to the other terms:

$$\tau_1 = \frac{1}{r_1}\left[r_i\tau_i - \alpha\frac{(r_i^2 - r_1^2)}{2}\right] \tag{7}$$

$$\tau_i = \tau_2\frac{r_2}{r_i}\frac{R_1}{R_2} \tag{8}$$

$$\tau_2 = \beta\frac{(r_m^2 - r_2^2)}{2r_2} \tag{9}$$

where

$$\alpha = \left(\frac{dP}{dx} + \frac{\rho_L g}{g_c}\right) \text{ and } \beta = \frac{dP}{dx} + \frac{\rho_G g}{g_c}$$

If the pressure gradient, point of maximum velocity, film thickness, and shear stress at the outer wall are known, the shear stress at the solid-liquid interface (τ_i) may be calculated and compared with values obtained via independent measurements.

Generally, entrainment is present for most two phase gas-liquid film flows. Equations (6) through (9) may still be used to estimate two phase flow parameters if the density of the gas core is available from entrainment data. For such a case

$$\frac{1}{\rho} = X\left(\frac{1}{\rho_G}\right) + (1-X)\left(\frac{1}{\rho_L}\right) \tag{10}$$

where X is the quality (weight fraction) of the gas phase. Since entrainment data is not available for the present system, no relation involving the density of the gas core was used for calculations in this work.

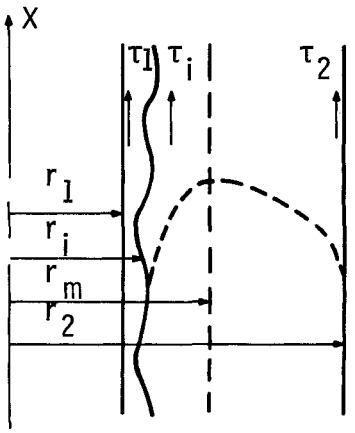

Fig. 1. Section of annular duct showing climbing film.

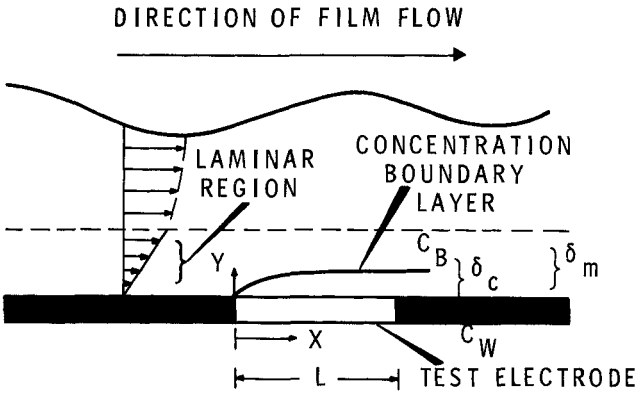

Fig. 2. Mass transfer at the solid-liquid interface.

Mass Transfer at the Solid-Liquid Interface

Consider the liquid film as shown in Figure 2 flowing over a smooth test electrode under the following conditions: (a) the liquid properties are constant; (b) the surface concentration is uniform ($c_w = 0$); (c) the undisturbed liquid bulk concentration is c_b; (d) mass transfer is due to diffusion alone; (e) surface curvature is negligible; (f) the test electrode is short (for small values of y, $\partial^2 c/\partial x^2 <<< \partial^2 c/\partial y^2$); (g) the concentration boundary layer is within the laminar sublayer which is fully developed; (h) the thickness of the concentration boundary layer is small compared to the mean film thickness; and (i) the velocity of the liquid near the wall is $u = \bar{a}y$, $v = 0$, $w = 0$.

This boundary value problem was solved by Leveque (*15*). The average mass transfer coefficient over a length, L, is:

$$\bar{k}_c = 1.68\ D_{AB}\left(\frac{\bar{a}}{9D_{AB}L}\right)^{1/3} \tag{11}$$

By using this relation one can estimate the momentum transfer to the inner core wall by means of experimental mass transfer data. This analysis is applicable to both laminar and turbulent liquid film flows provided the concentration boundary layer does not greatly exceed the region of linear velocity gradient near the wall.

Velocity Gradient and Shear Stress at the Solid-Liquid Film Interface

Rearrangement of Equation (11) gives the following expression for the velocity gradient in the region of the wall:

$$\bar{a} = 1.898\ D_{AB}L\left(\frac{\bar{k}_c}{D_{AB}}\right)^3 \tag{12}$$

If very short sections are considered, all mass transfer may occur within a relatively thin laminar layer of fluid near the wall. In such a case the concentration boundary layer would not extend beyond the so-called "laminar sublayer." Mass transfer coefficient measurements for short electrodes of different sizes are used to determine $\bar{a}$. If values for $\bar{a}$ for the different electrodes remain essentially constant under the same gas-liquid flow conditions, then the concentration boundary layer is within the laminar sublayer. In this case shear stresses at the inner wall may be calculated as follows:

$$\tau_1 = \frac{\mu}{g_c}\left(\frac{du}{dy}\right)_{y=0} = \frac{\mu\bar{a}}{g_c} \tag{13}$$

and

$$\tau_1 = \frac{1.898\mu D_{AB}L}{g_c}\left(\frac{\bar{k}_c}{D_{AB}}\right)^3 \tag{14}$$

Therefore shear stresses at the inner wall may be deter-

mined from electrode length, physical properties and experimental mass transfer coefficients calculated from Equation (2).

Estimation of Mean Interfacial Shear Stress

Equation (7) gives:

$$\tau_i = \frac{1}{r_i}\left[r_1\tau_1 + \alpha\frac{(r_i^2 - r_1^2)}{2} \right]$$

where τ_i is the mean interfacial shear stress which consists both of viscous drag and form drag on the air-liquid interface. Substitution of τ_1 from Equation (14) gives:

$$\tau_i = \frac{1}{r_i}\left[\frac{1.898\mu D_{AB} L r_1}{g_c}\left(\frac{k_c}{D_{AB}}\right)^3 + \alpha\left(\frac{r_i^2 - r_1^2}{2}\right) \right] \quad (15)$$

If the pressure gradient, film thickness, and mass transfer coefficient are known, τ_i may be determined.

The mean interfacial shear stress may also be determined using Equation (8) if the film thickness, point of maximum air velocity, and shear stress at the outer wall are known.

Estimation of Incipient Downflow

At very low gas flow rates insufficient momentum is transferred from the gas phase to the liquid film to maintain climbing film flow. Near the inner core wall the liquid film may be flowing downward even though the net liquid flow may be upward. Downflow begins when the shear stress at the solid-liquid interface is zero. From Equations (7) and (8):

$$0 = 2R_1 r_2 \tau_2 - \alpha R_2 (r_i^2 - r_1^2) \quad (16)$$

If the pressure gradient, point of maximum velocity, film thickness, and shear stress at the outer wall are known, downflow conditions may be estimated and compared with downflow results determined from experimental mass transfer measurements.

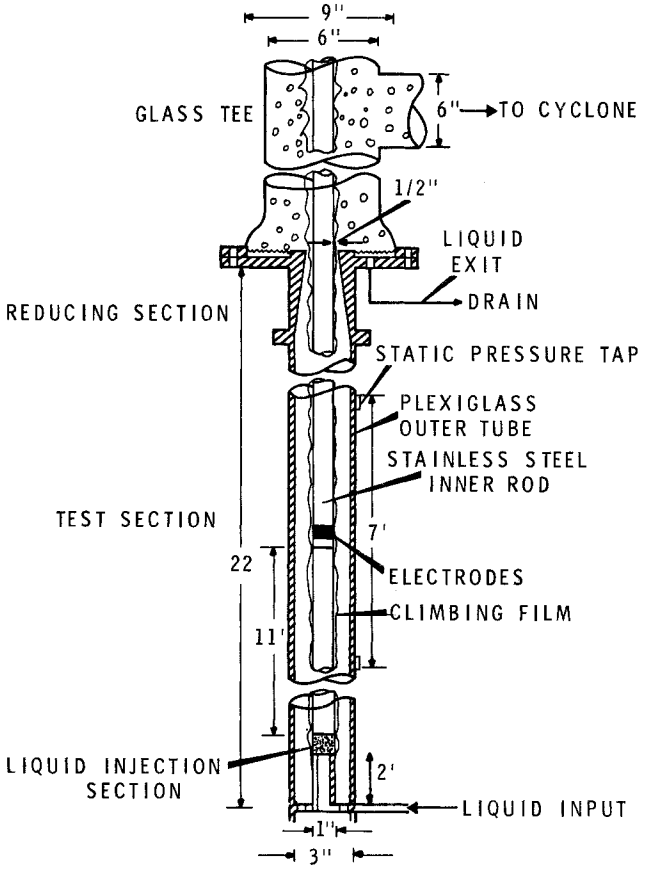

Fig. 3. Two phase flow column.

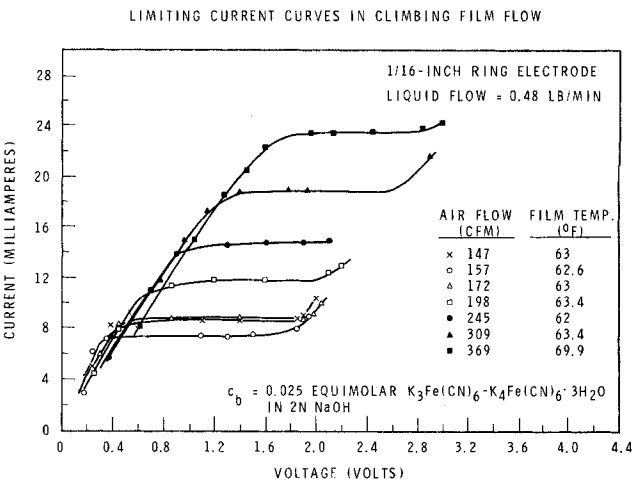

Fig. 4. Limiting current curves in climbing film flow.

EXPERIMENTAL APPARATUS AND PROCEDURE

Two Phase Flow System

A detailed sketch of the test section is presented in Figure 3. Cooled, metered air was supplied to the system by a blower rated at 550 cfm at 9 lb./sq. in. gauge. The vertical annular column was 35 ft. long including a 20 ft. long annular test section. The test section consisted of a 3 in. I.D. plexiglass tube with a 1 in. O.D. stainless steel concentric inner core that was supported laterally by sets of streamlined stainless steel centering screws.

The liquid supply was kept in a 15 gal. stainless steel, steam jacketed vessel and maintained under a nitrogen atmosphere. Liquid was pumped into the inner core of the annular column and entered the test section by a liquid injection section which consisted of a 1 in. O.D. stainless steel porous tube 2 in. long and 3/64 in. thick. Liquid was transported upwards as a thin film on the inner tube by means of momentum transferred from the air stream. The mass transfer measurement location was approximately 11 ft. above the liquid injector. At this location the liquid film temperature was also measured by means of a calibrated temperature probe. At the end of the column the air and liquid were completely separated by means of a reducing section and a subsequent cyclone arrangement. The liquid was subsequently discarded to drain.

Air flow rates 140 to 385 cfm at 68°F. and one atm., and liquid flow rates 0.2 to 1.46 lb./min. were investigated.

Electrochemical Systems

All experimental mass transfer data were obtained at limiting current which was determined from a plot of average current vs. potential similar to the curve in Figure 4. Limiting current was obtained at the flat portion of the curve. A potential was applied between the anode and the cathode, and the current in the circuit was measured. Adjustment of a rheostat in the circuit permitted the determination of the entire polarization curve.

Fluctuations in the electrochemical circuit current were recorded as voltage variations across standard resistors either by a Honeywell model 1508 visicorder or by a Tektronix type 545A oscilloscope. A Tektronix type 122 AC-coupled preamplifier with differential input was used in the circuit to amplify the voltage signal from the standard resistor. The common mode rejection ratio of this amplifier was used to eliminate the d.c. component. Adjustment of the high and low frequency response positions of the amplifier and subsequent observation of the oscilloscope trace allowed the determination of the frequency range of the signal.

The test electrodes were of two types, ring electrodes and wire electrodes. Both types of electrode assemblies constituted a portion of the inner core of the annular test section.

For the ring type of electrode, the electrochemical reaction was carried out between a large nickel ring (anode) and the small nickel ring (cathode) mounted flush to the inner core wall. The 1 in. long anode was sufficiently large so that the current was not limited in any way. Thus, all concentration

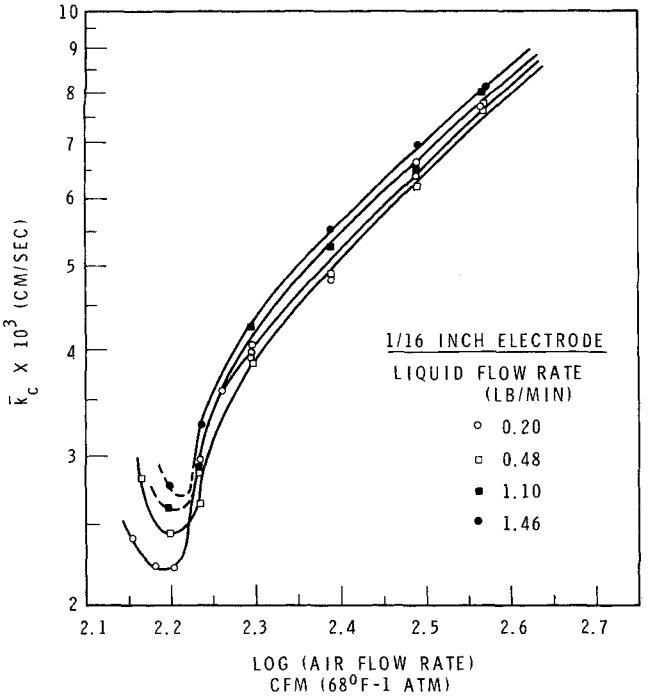

Fig. 5. Mass transfer coefficient vs. air flow rate.

polarization effects were due only to the reaction at the cathode. The cathodes varied in length from approximately 1/16 to 1/8 in. long. The primary purpose of this ring type of electrode assembly was to measure average mass transfer coefficients as a function of liquid and gas flow rates.

The electrode rings were mounted concentrically onto an approximately 1 in. O.D. plexiglass rod which had been machined and threaded on each end to ⅝ in. O.D. (*26*). A ½ in. long plexiglass spacer separated the electrodes. Epoxy cement was applied to the electrodes and spacer; immediately afterwards, a ½ in. long plexiglass spacer was screwed firmly against the anode to hold the electrodes in place. This spacer also insulated the anode from the upper section of the inner core. Each electrode assembly was constructed so that a minimum of 3 in. of smooth plexiglass preceded the test electrode (cathode) in order to eliminate disturbing the flow field near the core wall. The entire electrode assembly was machined in one operation to the dimensions of the inner core and polished smooth with rouge paper.

Prior to the installation of the electrodes in the system, they were cleaned with carbon tetrachloride. Each electrode remained in the system for a series of experiments. Before each experimental run the electrodes were cathodically cleaned in 5% sodium hydroxide solution at a current density of 20 ma. for 12 to 15 min. to minimize chemical polarization effects (*6, 20*). Following each run the cell was inspected to ascertain if adverse corrosion deposits had formed on the electrode surface during the experiment. In general, no such deposits were formed during the experimental runs if the aforementioned cleaning procedure was followed. Failure to properly clean the electrodes causes erroneous mass transfer results (*27*). Care was also taken to operate the cell no longer than 3 hr. without recleaning the electrodes.

The wire type of electrode assembly was essentially the same as the ring type of assembly except for the cathode design. The cathode was a 0.064 in. diameter nickel wire mounted flush to the inner core wall. The wire was inserted into the plexiglass spacer separating it from the anode and was held in place with epoxy cement. The entire electrode assembly was machined and polished to its proper dimensions after all components had been assembled. This type of electrode arrangement was utilized to obtain velocity gradient fluctuations at the solid-liquid film interface.

For all climbing film flow experiments the electrolyte used was a 0.025 equimolar solution of potassium ferricyanide and potassium ferrocyanide in 2*N* sodium hydroxide. The sodium hydroxide acted as an indifferent electrolyte to eliminate any migration due to ionic transference effects. The solutions were prepared just prior to the runs using distilled water which had been purged with nitrogen to eliminate dissolved oxygen. Precautions were taken to keep the test solution away from light.

EFFECT OF DISSOLVED OXYGEN

In a preliminary study (*26, 27*) suitable dissolved oxygen limits were established for the electrochemical measurement of mass transfer coefficients in the presence of air. This study showed that if the test solution is first saturated with nitrogen, future exposure to air for a short period of time does not greatly affect the mass transfer data.

In the climbing film flow study the electrolyte was completely saturated with nitrogen prior to its injection into the annular test section. The solution in the liquid reservoir was maintained at approximately 10% saturation. The percentage of dissolved oxygen in the redox solution increased as it flowed upward through the two phase system. The dissolved oxygen content of the climbing film was measured about 6 in. above the test electrodes, and for the liquid and gas flow rates studied the percent saturation of dissolved oxygen at this location varied between 30 to 50%. Based on previous results (*26, 27*) the effect of dissolved oxygen on the mass transfer coefficient in this climbing film flow study is less than 2%. All dissolved oxygen content measurements were obtained with a Beckman Oxygen Analyzer model 777.

EXPERIMENTAL RESULTS

Mass Transfer Coefficients at the Solid-Liquid Film Interface

Figures 5 to 6 summarize the experimental data for the 1/16 in. electrode. Figure 5 presents $\bar{k}_c$ as a function of air flow rate with liquid flow rate as parameter, whereas, Figure 6 presents $\bar{k}_c$ as a function of liquid flow rate with air flow rate as parameter. The data are plotted in this

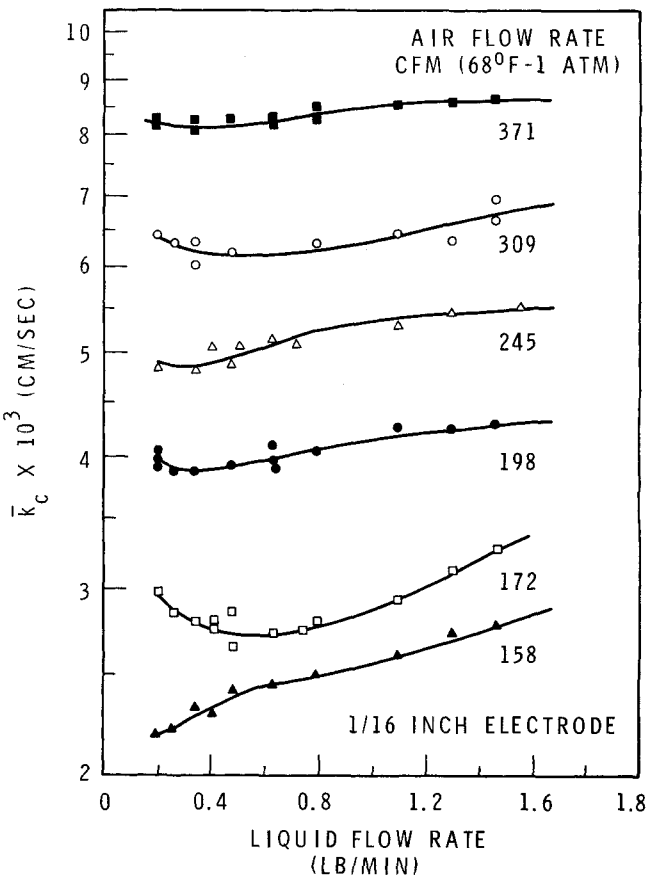

Fig. 6. Mass transfer coefficient vs. liquid flow rate.

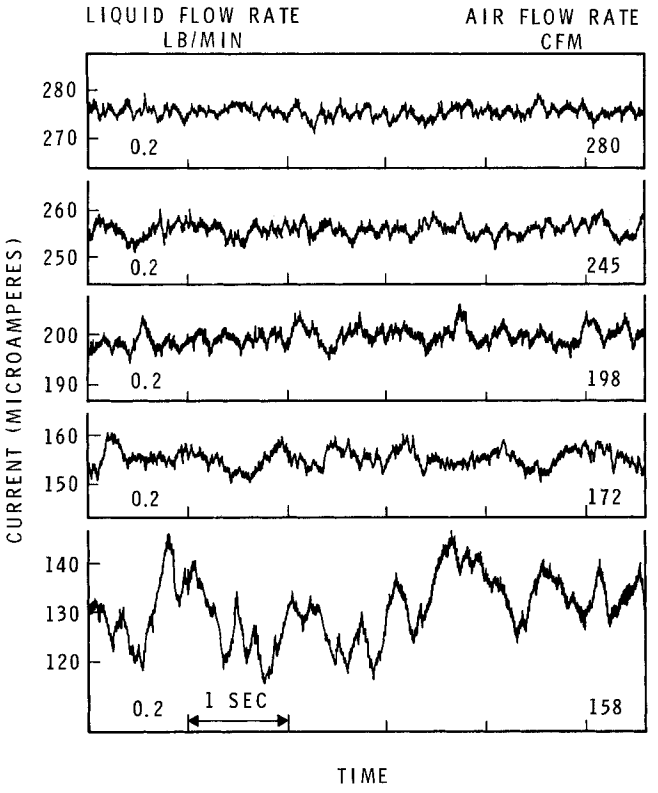

Fig. 7. Fluctuations in the rate of mass transfer at the solid-liquid film interface.

manner in order to examine the relative effects of air and liquid flow rates on the mass transfer process. The experimental mass transfer coefficients are considered accurate to within ±5%.

Data were also obtained with a ⅛ in. electrode to make certain that the experimental velocity gradients were satisfactory. Good agreement between the two electrodes was obtained. The data of the 1/16 in. electrode are more extensive than those of the ⅛ in. electrode; hence, reference will be made primarily to the data of the shorter electrode.

Figure 5 shows the dependence of $\overline{k_c}$ on gas flow rate. The mass transfer coefficient decreases rapidly as the air flow rate is decreased at constant liquid flow rate. As the gas flow rate decreases the film thickness increases, and the film velocity decreases; thus, $\overline{k_c}$ decreases. At very low gas flow rates $\overline{k_c}$ exhibits a minimum value which corresponds to incipient downflow within the film. Although the shear stress at the inner wall is zero at incipient downflow, $\overline{k_c}$ has a finite value. Since the film is very agitated at this point, $\overline{k_c}$ is probably much greater than it would be under stagnant conditions. As flooding is approached $\overline{k_c}$ increases slightly due to increased downflow and agitation within the film.

Figure 6 shows the effect of liquid flow rate on $\overline{k_c}$. Except for the lowest gas flow case, the nature of the relationship between $\overline{k_c}$ and liquid flow is qualitatively the same regardless of gas flow rate. The mass transfer coefficient decreases slightly as liquid flow rate is decreased. At low liquid flow rates, $\overline{k_c}$ increases sharply just before the minimum wetting rate is reached. The rise in $\overline{k_c}$ just prior to the minimum wetting rate is caused not only by a decrease in film thickness but also by turbulence developed in the film during the groping and reforming periods. A similar rise in heat transfer coefficient near the minimum wetting rate region was measured by Norman and McIntyre (*19*) for a falling liquid film on a vertical surface.

The lowest gas flow rate in Figure 6 corresponds to the downflow region. In this low film velocity region the film tends to maintain its identity at lower liquid rates and the minimum wetting rate is lowered. Therefore, no rise in $\overline{k_c}$ was noted in the low liquid flow range.

A comparison of Figures 5 and 6 shows the mass transfer coefficient is much more dependent on air flow rate than on liquid flow rate primarily because film velocity, film thickness, and film stability are strongly dependent on the gas flow rate.

Fluctuations in Rate of Mass Transfer to a Wire Electrode

Visicorder traces of the fluctuations in the rate of mass transfer to a small wire electrode are shown for various flow conditions in Figure 7. The frequencies of the fluctuations are mostly in the 0.2 to 100 cycles/sec. range although a power spectrum density analysis is required to describe in detail the frequency domain of the signals. The intensity of the fluctuations increases as the gas flow rate is decreased. At downflow conditions the fluctuations increase considerably indicating a transition in the flow field near the electrode. For the same gas flow rate the film is more stable at low liquid flow rates than at high liquid flow rates. Since more momentum transfer from the air stream is required to maintain high liquid flow films, this result is to be expected.

The present data indicate that mass transfer at the solid-liquid wall may be influenced by the wave structure of the climbing film. The visicorder traces for downflow reflect to a considerable degree the observed pulse-by-pulse nature of the climbing film under downflow conditions. Similar results have been shown by Chand and Rosson (3) who demonstrated the importance of wave motion on the heat transfer process within a falling film. Further instantaneous local measurements are required to study the quantitative effect of the air-liquid interface on the rate of mass transfer to the inner wall, and to classify flow regimes which occur in climbing film flow (*5*).

Velocity Gradients at the Solid-Liquid Interface

A comparison of the velocity gradients at the solid-liquid film interface calculated from experimental mass transfer data of the 1/16 in. and ⅛ in. electrodes for the same air and liquid flow was made. The average calculated value of $\overline{a_1}/\overline{a_2}$ was 1.35. If the ratio $\overline{a_1}/\overline{a_2}$ is approximately 1.0,

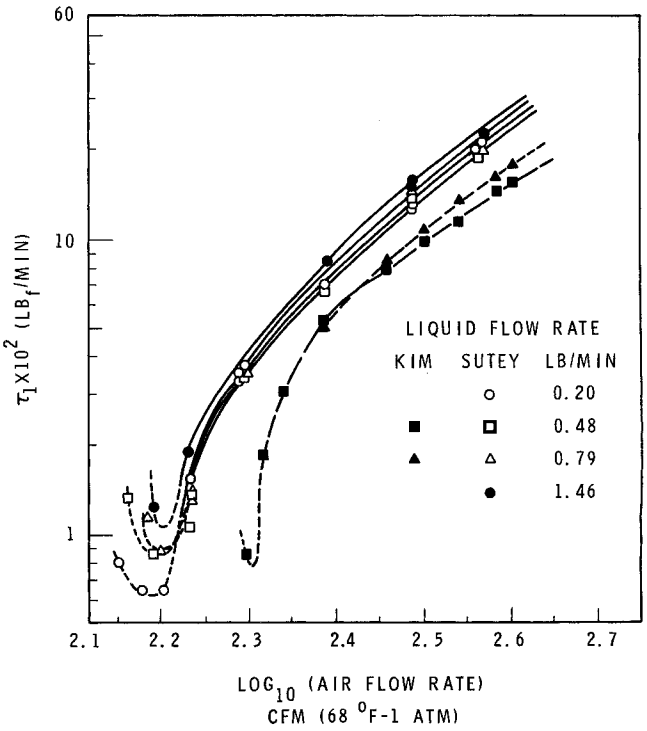

Fig. 8. Shear stress at the solid-liquid film interface.

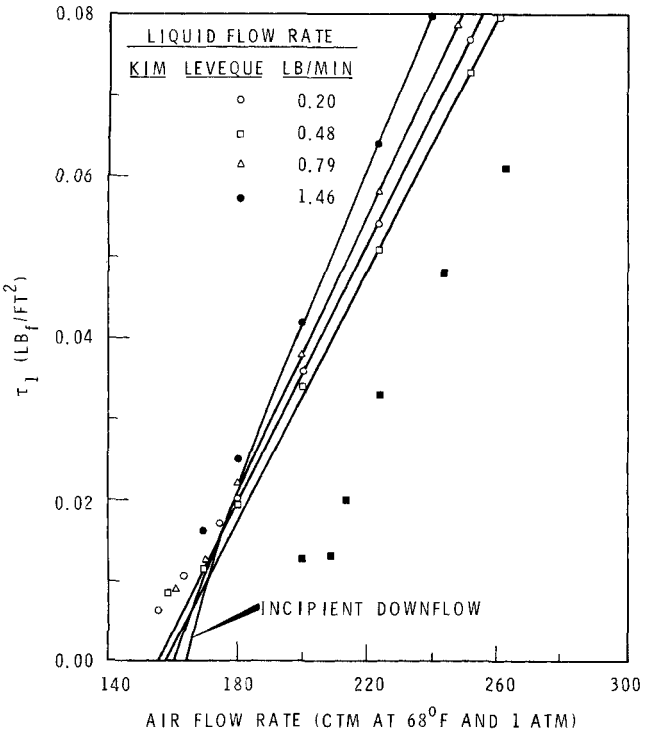

Fig. 9. Shear stress at the solid-liquid film interface at downflow.

all mass transfer measurements are assumed to occur within a region of uniform velocity gradient close to the inner wall. This comparison between $\bar{a}_1$ and $\bar{a}_2$ is reasonably good and well within experimental error. Since $\bar{a}_1/\bar{a}_2$ is dependent of $(D_2/D_1)^2$ $(\bar{k}_{c_1}/\bar{k}_{c_2})^3$ a small error in the values of $\bar{k}_c$ and D could cause a large error in the calculated value of $\bar{a}_1/\bar{a}_2$. To further ensure that all mass transfer measurements were obtained within a laminar flow region near the wall, only the experimental data of the 1/16 in. electrode were used to calculate other quantities based on the Leveque model.

Based on the classical film model ($\delta = D/\bar{k}_c$), the concentration boundary layer thickness was determined from mass transfer coefficient data for the 1/16 in. electrode. The estimated concentration boundary layer thickness was 4 to 9% of the experimental liquid film thickness for liquid flows of 0.48 to 0.79 lb./min. and gas flows of 198 to 379 cfm. Thus, under these conditions the Leveque model is applicable.

Shear Stress at the Inner Wall

The shear stress at the solid-liquid interface was calculated from Equation (14) by means of experimental mass transfer data for the 1/16 in. electrode. The accuracy of τ_1 is estimated to be within ± 20%. In Figure 8, τ_1 is presented as a function of gas flow rate with liquid flow rate as parameter and as would be expected exhibits a character similar to $\bar{k}_c$.

The minimum value of τ_1 in Figure 8 corresponds to incipient downflow within the film even though τ_1 is not zero. This results since $\bar{k}_c$ is finite at incipient downflow. Also, since $\bar{k}_c$ is always positive, only positive τ_1 values are predicted. Nevertheless, the minimum value of τ_1 indicates a transition in the velocity gradient at the wall. For gas flow rates less than 180 cfm, the actual shear stresses were obtained by extrapolation of the lines shown in Figure 9. It is noted that zero shear stress occurs in the region 155 to 165 cfm.

Values of τ_1 were also calculated from Equations (7) and (8). Film thicknesses, shear stresses at the outer wall, and radii of maximum air velocity obtained by Kim (*13, 14*) were used with pressure gradients from the present work. These results are also presented in Figure 9 and are within 25 to 60% of those obtained by using $\bar{k}_c$ data. The discrepancy between τ_1 values predicted by the two sets of data may be attributed in part to errors in mean film thickness reported by Kim (*13, 14*). Errors in mean film thickness cause appreciable errors in values of τ_1 values calculated from Equations (7) and (8). The greatest deviation in predicted τ_1 values occurs in the low air flow rate region where the data of Kim are minimal. Additional accurate film thickness data are required in the low air flow rate region to explain these differences.

Pressure Gradient and Entrainment

Typical pressure gradients are presented in Figure 10 as a function of air flow rate with liquid flow rate as parameter. Except at very low air flow rates the effect of entrainment on the pressure gradient is negligible for the flow rates studied. At very low air flow rates the pressure gradient reaches a minimum value which closely corresponds in terms of air and liquid flow rates to incipient downflow as shown by $\bar{k}_c$ data in Figure 5. Under downflow conditions the air-liquid interface is very rough and unstable requiring more energy to be transferred from the air to maintain the climbing film. Thus, the pressure gradient increases as flooding is approached.

Shear Stress at the Air-Liquid Interface

The shear stress (τ_i) at the air-liquid film interface was calculated from Equation (7) using τ_1 and α values determined in the present study and mean film thickness data of Kim (*13, 14*).

In Figure 11, τ_i is presented as a function of gas flow rate with liquid flow rate as parameter. The interfacial shear stress decreases as gas flow rate decreases. For a liquid flow rate of 0.48 lb./min. for which film thickness data is available, τ_i exhibits a minimum value at a gas flow rate of 224 cfm, whereas, downflow occurs at 158 cfm based on $\bar{k}_c$ data. The increase in τ_i at low gas flows is due to the concurrent increase in the roughness and thickness of the liquid film. The minimum of τ_i signals the gradual change of the velocity gradient at the inner wall from positive to negative. Further study in light of additional film thickness data is required to explain the behavior of τ_i.

Values of τ_i were also calculated from Equation (8). Film thickness, shear stresses at the outer wall, and radii of maximum air velocity obtained by Kim (*13, 14*) were used. These results are also presented in Figure 11 and compare within 20 to 40% of those obtained with present results.

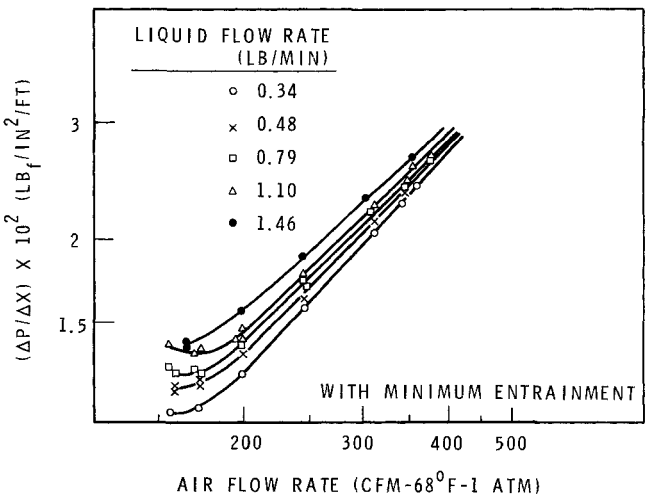

Fig. 10. Pressure gradient vs. air flow rate at minimum entrainment.

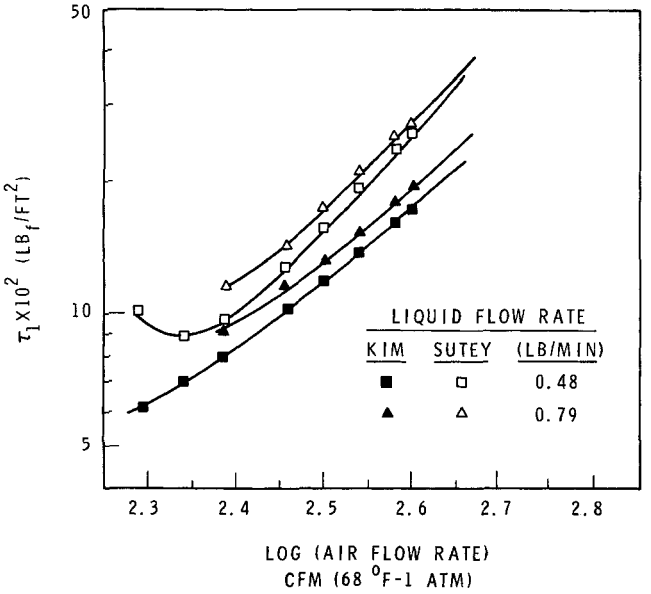

Fig. 11. Interfacial shear stress vs. air flow rate.

DISCUSSION OF RESULTS

The instantaneous local measurements of mass transfer at the solid-liquid interface permit better understanding of the nature of climbing film flow. In their studies of electrochemical mass transfer to a small electrode on a pipe wall, Reiss and Hanratty (*21*) recorded no fluctuations in the rate of mass transfer to the electrode in the laminar flow regime. At a Reynolds number of 2,140 a slight wavy disturbance was noted. These disturbances increased in the transition region and were observed to greatly increase in frequency and intensity as the Reynolds number further increased to fully developed turbulent flow conditions. Based on these observations of Reiss and Hanratty and the traces in Figure 7, climbing film flow is considered turbulent for the gas and liquid flows studied. The climbing film is relatively stable at high gas flow rates but becomes increasingly turbulent as the gas flow rate is decreased at a constant liquid flow rate. Turbulence is more characteristic of climbing films formed from high liquid flow rates than those formed from low liquid flow rates.

On the basis of the fluctuating mass transfer data obtained in this study, surface renewal models (*4, 9, 11, 28*) are considered as possible explanations of the exchange of heat, mass, and momentum transfer from the climbing film to the inner wall. Surface renewal parameters may be determined from the mass transfer results of this work and used to predict heat transfer results for the climbing film system. Since no convective heat transfer results are presently available for this system, surface renewal models were not tested.

Under downflow conditions, flow adjacent to the inner wall is downward even though the net flow of the film may be upward. At incipient downflow the shear stress at the inner wall is zero. The air and liquid flow conditions at incipient downflow are estimated at the minimum values of the mass transfer coefficient and pressure gradient. These values are presented in Table 1 and show excellent agreement with each other. Table 1 shows that incipient downflow occurs at progressively higher air flow rates as the liquid flow rate increases, since more momentum transfer from the air is required to maintain the higher liquid film flows. Predictions of incipient downflow by means of local mass transfer coefficient data are considered the most reliable and do not depend on subjective visual observations of the film.

Downflow may also be measured by the occurrence of

Table 1. Air Flow Rates at Incipient Downflow

Liquid Flow Rate, lb./min.	$\Delta P/\Delta x$ Minimum Entrainment	$\Delta P/\Delta x$ Equilibrium Entrainment	τ_1 From Mass Transfer Measurements	τ_1 Kim-Knudsen
	Air Flow Rate (cfm)—at 68°F. and 1 atm.			
0.20			156	
0.34	158	165	157	
0.48	158	160	158	202
0.79	164	168	161	
1.10	172	185	163	
1.30	170		164	
1.46			164	

high intensity fluctuations in the local instantaneous rate of mass transfer to a wire electrode as shown in Figure 7. However, insufficient data is presently available over a wide range of liquid flows to use this method.

Downflow was also observed by Willis (*29*) and Hewitt, et al. (*10*) in upward annular air-water flow in a vertical tube. Curves of pressure gradient vs. gas flow rate at constant liquid flow exhibited minimum values which corresponded to zero wall shear stress. Fair agreement was obtained between measured minimum pressure gradients and those predicted using laminar film flow theory.

The shear distribution within the film is described by Figure 12*a* in which the ratio of the interfacial shear to the shear stress at the inner wall is presented. At very low gas rates, τ_i/τ_1 approaches infinity as downflow is approached. At high gas rates this ratio becomes independent of liquid flow rate and approaches unity; that is, the shear stress is constant across the film. Shearer and Nedderman (*25*) have also reported $\tau_w = \tau_i$ (to a 1% accuracy) for the small ripple wave regime in annular climbing film flow.

The variation of τ_i/τ_1 with flow conditions, Figure 12*a* is closely related to that of mean film thickness with flow conditions as shown in Figure 12*b*. At very low gas rates the film thickness approaches infinity as downflow and flooding is approached. As the gas flow rate increases the film thickness decreases rapidly up to a flow rate of 240 cfm after which it decreases more slowly becoming nearly independent of liquid flow rate at the highest air flow studied. The similar behavior of τ_i/τ_1 and film thickness with flow conditions demonstrates the dependence of the velocity profile on film thickness.

CONCLUSIONS

The results of this study are as follows:

1. At constant liquid flow rate the mass transfer coefficient decreases rapidly as air flow rate decreases, and at very low gas flow rates exhibits a minimum value which corresponds to incipient downflow within the climbing film.

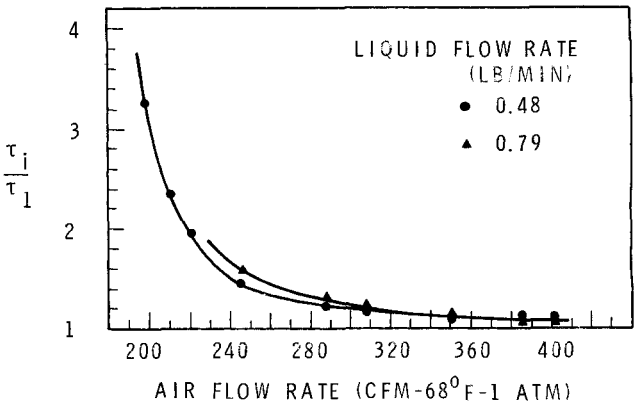

Fig. 12*a*. Shear stress distribution vs. air flow rate.

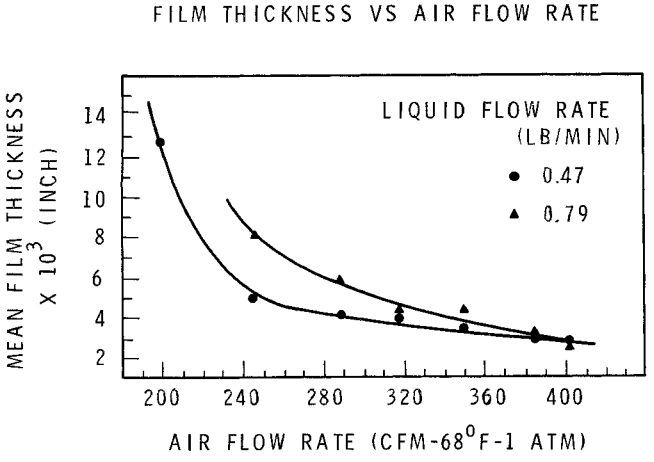

Fig. 12b. Film thickness vs. air flow rate.

2. At constant gas flow rate the mass transfer coefficient decreases slightly as liquid flow rate is decreased and at very low liquid flow rates increases sharply just prior to the minimum wetting rate.

3. Based on the fluctuations in the rate of mass transfer to the inner core wall, the climbing film flow is considered turbulent for the gas and liquid flows studied. The climbing film is relatively stable at high gas flow rates but becomes increasingly turbulent as downflow is approached.

4. The shear stress at the inner wall was calculated from the Leveque theory for climbing film flow by using experimental mass transfer data of a short electrode. Results compare well with independent values calculated from previous work.

5. At constant liquid flow rate the pressure gradient decreases rapidly as the air flow rate decreases and at very low air flow rates reaches a minimum value which closely corresponds, in terms of air and liquid flow rates, to incipient downflow as indicated by the mass transfer coefficient data.

6. Interfacial shear stresses were calculated from two separate relationships each using independent experimental data and the results compare well with each other.

7. At very low gas rates the shear stress ratio τ_i/τ_1 approaches infinity as downflow is approached. At high gas rates this ratio becomes independent of liquid flow rate and approaches unity. The similar behavior of τ_i/τ_1 and film thickness as affected by flow conditions demonstrates the dependence of the velocity profile on film thickness.

NOTATION

$\bar{a}$ = velocity gradient at the electrode wall, 1/sec.
A = surface area of working electrode, sq.cm.
c_b = bulk concentration of ferricyanide ions, moles/cc.
c_w = interfacial (solid-liquid) concentration, moles/cc.
D_{AB} = diffusivity of ferricyanide ions, sq.cm./sec.
F = Faraday (96,500), coulomb/equivalent
g = acceleration of gravity, ft./sq.sec.
g_c = force-mass conversion factor (32.17), lb.$_m$ft./lb.$_f$sq.sec.
i = current, amp.
i_L = limiting current, amp.
$\bar{k}_c$ = average mass transfer coefficient, cm./sec.
L = length of electrode, in.
Log = Logarithm to the base 10, dimensionless
n = number of electrons involved in electrode reaction
P = pressure, lb.$_f$/sq.ft.
$\Delta P/\Delta x$ = pressure gradient, lb.$_f$/cu.ft.
r = direction coordinate, in.
r_1 = inner core radius, in.
r_2 = outer tube radius, in.
r_i = interface (liquid film-air) radius, in.
r_m = radius of maximum air velocity, in.
R_1 = $(r_m^2 - r_i^2)/(r_2^2 - r_1^2)$, dimensionless
R_2 = $(r_2^2 - r_m^2)/(r_2^2 - r_1^2)$, dimensionless
R_L = $(r_i^2 - r_1^2)/(r_2^2 - r_1^2)$, dimensionless
R_G = $(r_2^2 - r_i^2)/(r_2^2 - r_1^2)$, dimensionless
u = local velocity in the x direction, ft./sec.
v = local velocity in r (or y) direction, ft./sec.
x, y = distance coordinate, in.
α = $(\Delta P/\Delta x + \rho_L g/g_c)$, lb.$_f$/cu.ft.
β = $(\Delta P/\Delta x + \rho_G g/g_c)$, lb.$_f$/cu.ft.
μ = viscosity, lb.$_m$/ft.sec.
ρ_L = density of liquid (electrolyte), lb.$_m$/cu.ft.
ρ_G = density of gas (air), lb.$_m$/cu.ft.
τ = shear stress, lb.$_f$/sq.ft.
τ_1 = shear stress at solid-liquid film interface (at inner core wall), lb.$_f$/sq.ft.
τ_2 = shear stress at outer tube wall, lb.$_f$/sq.ft.
τ_i = interfacial (air-liquid film) shear stress, lb.$_f$/sq.ft.
X = quality (weight fraction) of the gas phase, dimensionless

LITERATURE CITED

1. Bazan, J. C., and A. J. Arvia, *Electrochim. Acta*, **9**, 667 (1964).
2. *Ibid.*, **10**, 1025 (1965).
3. Chand, R., and H. F. Rosson, *Ind. Eng. Chem. Fundamentals*, **4**, 356 (1965).
4. Danckwerts, P. V., *ibid.*, **43**, 1460 (1951).
5. Dukler, A. E., and M. G. Hubbard, *Proc. Heat Transfer Fluid Mech. Inst.*, Univ. Santa Clara, 100 (June, 1966).
6. Eisenberg, M., C. W. Tobias, and C. R. Wilke, *Trans. Electrochemical Soc.*, **101**, 306 (1954).
7. Glasstone, S., "Introduction to Electrochemistry," Van Nostrand, New York (1942).
8. Grassman, P., *Chem. Ing. Teck.*, **8**, 529 (1961).
9. Hanratty, T. J., *AIChE J.*, **7**, 488 (1961).
10. Hewitt, G. F., P. M. C. Lacey, and B. Nicholls, *U. K. At. Energy Authority, AERE-R-4614*, p. 35 (1965).
11. Higbie, R. Trans. *AIChE*, **31**, 365 (1935).
12. Iribarne, I., A. D. Gosman, and D. B. Spalding, *Int. J. Heat Mass Transfer*, **10**, 1661 (1967).
13. Kim, D. H., Ph.D. thesis, Oregon State Univ., Corvallis (1965).
14. Kim, D. H., and J. G. Knudsen, *AIChE J.*, **13**, 326 (1967).
15. Knudsen, J. G., and D. L. Katz, "Fluid Dynamics and Heat Transfer," New York, McGraw-Hill (1958).
16. Kolthoff, I. M., and E. A. Pearson, Ind. Eng. Chem., **3**, 381 (1931).
17. Lin, C. S., E. B. Denton, N. S. Gaskill and G. L. Putnam, **43**, 2136 (1966).
18. Mitchell, J. E., and T. J. Hanratty, *J. Fluid Mechanics*, **26**, 199 (1966).
19. Norman, W. S., and V. McIntyre, *Trans. Inst. Chem. Eng., London*, **38**, 301 (1960).
20. Petrocelli, J. V. and A. A. Paolucci, *J. Electrochem. Soc.*, **98**, 291 (1951).
21. Reiss, L. P., and T. J. Hanratty, *AIChE J.*, **8**, 245 (1962).
22. *Ibid.*, **9**, 154 (1963).
23. Shaw, P. V., and T. J. Hanratty, *AIChE J.*, **10**, 475 (1964).
24. ———, L. P. Reiss, and T. J. Hanratty, *ibid.*, **9**, 362 (1963).
25. Shearer, C. J., and R. M. Nedderman, Chem. Eng. Sci., **20**, 671 (1965).
26. Sutey, A. M., Ph.D. thesis, Oregon State Univ., Corvallis (June, 1967).
27. ———, and J. G. Knudsen, *Ind. Eng. Chem. Fundamentals*, **6**, 132 (1967).
28. Toor, H. L., and J. M. Marchello, *AIChE J.*, **4**, 97 (1958).
29. Willis, I. J., *Chem. Eng. Sci.*, **20**, 895 (1965).

Manuscript received November 17, 1967; revision received April 29, 1968; paper accepted May 1, 1968. Paper presented at AIChE Tampa meeting.